Femtosecond laser trapping nanoprinting of silver micro/nanostructures

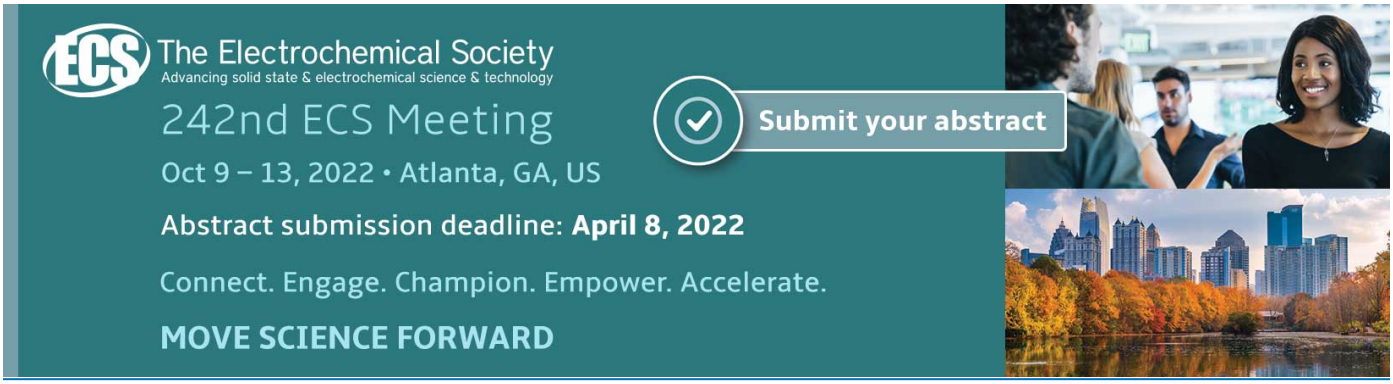

IOP Publishing Nanotechnology
Nanotechnology 32 (2021) 505303 (6pp) https://doi.org/10.1088/1361-6528/ac297f

Femtosecond laser trapping nanoprinting of silver micro/nanostructures

Zhong-Yun Chen[1,2,5], Hong-Zhong Cao[3,5,*], Liang-Cheng Cao[2], Gan Fang[2] and Xuan-Ming Duan[4,*]

[1] Chongqing Key Laboratory of Additive Manufacturing Technology and Systems, Chongqing Institute of Green and Intelligent Technology, Chinese Academy of Sciences, Chongqing 400714, People's Republic of China
[2] Key Laboratory of Airborne Optical Imaging and Measurement, Changchun Institute of Optics, Fine Mechanics and Physics, Chinese Academy of Sciences, Changchun 130033, People's Republic of China
[3] Shandong Provincial Key Laboratory of Laser Polarization and Information Technology, Laser Institute, Qufu Normal University, Qufu 273165, People's Republic of China
[4] Guangdong Provincial Key Laboratory of Optical Fiber Sensing and Communications, Institute of Photonics Technology, Jinan University, Guangzhou 510632, People's Republic of China

E-mail: hzcao@qfnu.edu.cn and xmduan@jnu.edu.cn

Received 9 July 2021, revised 10 September 2021
Accepted for publication 23 September 2021
Published 13 October 2021

Abstract

In this paper, silver micro/nanostructures composed of sintered nanoparticles were printed by capturing silver nanoparticles in water with 800 nm femtosecond laser trapping. Relationships of laser power, scanning speed, nanoparticle concentration, and the width and morphology of fabricated silver wire were systematically investigated. It is found that low scanning speed and high nanoparticle concentration favor the printing of silver wire with good morphology. A silver wire with width of 305 nm was printed. Electrical resistivities of printed wires are about 24 times that of bulk silver. Silver grid structures and dot arrays were printed by using this technology. Several three-dimensional silver cuboid structures were also printed. This work provides a protocol for printing of three-dimensional metallic micro/nanostructures using laser trapping. These printed structures have great application prospects in metamaterials, flexible electronics, and SERS.

Supplementary material for this article is available online

Keywords: laser nanoprinting, laser trapping, laser micro/nanofabrication, femtosecond laser, three-dimensional silver micro/nanostructures

(Some figures may appear in colour only in the online journal)

1. Introduction

Because of the excellent physical and chemical properties of metal, metallic micro/nanostructures have been playing important roles in micro/nanoelectronics [1, 2], MEMS [3, 4], surface plasmonics focusing and propagating [5, 6], metamaterials [7], SERS [8, 9], etc. Therefore, fabricating technologies of metallic micro/nanostructures have attracted increasing attentions. Metallic micro/nanostructures are usually fabricated by combining lithography of photoresist with metal deposition [10, 11]. However, this fabricating process is complex and inefficient. Therefore, a variety of direct writing technologies for metallic micro/nanostructures have been developed in the past decades, for example, inkjet printing [12], electron beam deposition [13], two-photon polymerization with metal nanoparticles [14, 15], and multi-photon photo-reduction [16, 17]. Laser trapping nanoprinting is a technology which can fabricate micro/nanostructures by using simple theory, process and instrument. Bahns *et al* and Xu *et al* reported printing of C-Au [18] and Au [19] structures using this technology, respectively. The optimal spatial

[5] These authors contributed equally to this work.
[*] Authors to whom any correspondence should be addressed

resolution was about 600 nm. Wang *et al* have printed silver micro/nanostructures composed of assembled nanoparticles [20]. However, morphologies of printed structures still need to be improved. Influencing mechanisms of different fabricating parameters, especially scanning speed and nanoparticle concentration, have not been systematically investigated. Compared with two-dimensional metallic micro/nano-structures, three-dimensional metallic micro/nanostructures have extraordinary and significant applications in metamaterials [21] and MEMS [11]. Laser printing has been a powerful fabrication technology for three-dimensional macroscopic metallic structures [22]. However, laser trapping nanoprinting of three-dimensional micro/nanostructure has not been realized. In this paper, silver nanowires composed of sintered nanoparticles were directly written by using femtosecond laser trapping nanoprinting (FLTN) with an 800 nm femtosecond laser. Influences of laser power, scanning speed, and silver nanoparticle concentration on wire width and wire morphology were studied systematically. A silver wire with width of 305 nm was written. Electrical resistivities of the fabricated silver wires are about 24 times that of bulk silver. Several two-dimensional silver structures were fabricated by using this technology. Three-dimensional silver cuboid microstructures were also printed. This study provides an evidence for fabricating metallic micro/nanostructures, especially three-dimensional micro/nanostructures, by using FLTN.

2. Experimental setup and theoretical calculations

The silver nanoparticle solution used in this work was prepared according to a reported method (detailed process is provided in section 1 of supplementary material 1) [23]. The concentration of the final silver nanoparticle aqueous solution is about 100 mg ml^{-1}, and sizes of silver nanoparticles are about 13 nm (figure S1 in supplementary material 1 (available online at stacks.iop.org/NANO/32/505303/mmedia)). Figure 1(a) shows the schematic diagram of FLTN experimental setup. A Ti: sapphire femtosecond laser (Spectra Physics, MaiTai HP, 100 fs, 80 MHz) with a center wavelength of 800 nm was employed as the light source. Laser beam coming from this source was expanded by lens group of lens 1 and lens 2, and reflected by mirror 2. The reflected beam entranced a high numerical aperture oil-immersed objective (Olympus, 100×, 1.49) and was tightly focused onto the interface of glass substrate and silver nanoparticle solution. A shutter and an attenuator were placed in the light path to switch the laser beam and adjust the laser power, respectively. A three-dimensional piezostage (Physik Instrumente, P-563.3CD) was used to realize the accurate movement in the experiment. The shutter, attenuator and piezostage were all controlled by a computer. In order to avoid solvent volatilization during the experimental process, a piece of adhesive film was cut out a square groove with size of about 10 mm × 10 mm and tied on the glass substrate. The silver nanoparticle solution was added in the square groove and covered by a coverslip.

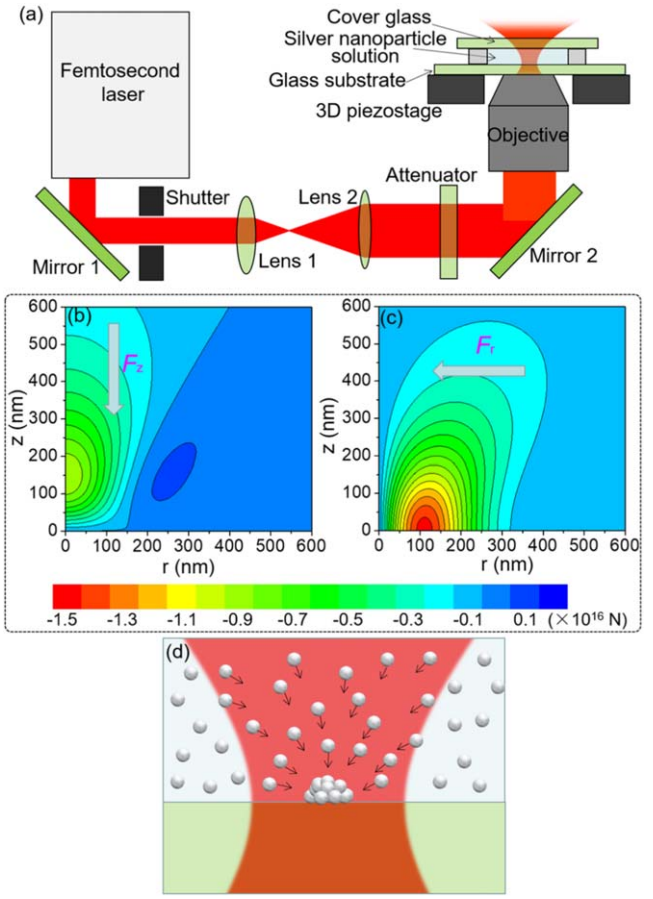

Figure 1. (a) Schematic diagram of main experimental setup for FLTN; (b) resultant force in vertical direction caused by laser light with measured power of 1 mW; (c) resultant force in radial direction caused by laser light with measured power of 1 mW; (d) schematic diagram of trapping and nanoprinting process for FLTN.

In solution, there are electrostatic repulsive force F_e and Van der Waals attractive force F_v between neighboring nanoparticles. For nanoparticles in incident light, there are also optical gradient force F_g, absorption force F_a, and scattering force F_s. As shown in the figure 1(a), the light irradiates the solution from glass substrate. Therefore, the gradient force F_g is the trapping force driving nanoparticles move to the laser focal point, and absorption force F_a and scattering force F_s are adverse forces causing nanoparticles go away from the laser focal point. Because laser power is small in the experiment, the Kerr effect could be ignored. Light-nanoparticle interaction of the femtosecond laser was equal to that of a CW laser with the same average power. The gradient force F_g, absorption force F_a, scattering force F_s can be expressed by $F_g = \frac{|\alpha|}{2} n_w{}^2 \varepsilon_0 \nabla \langle E^2 \rangle$, $F_s = \frac{n_w}{c} I C_{scat}$, and $F_a = \frac{n_w}{c} I C_{abs}$ (see section 2 of supplementary material 1) [24, 25]. The F_g can be divided into $F_{g,r}$ and $F_{g,z}$, which are gradient forces in radial and vertical axis, respectively. For a silver nanoparticle with the diameter of 13 nm near the laser focus center of the tightly focused 800 nm laser beam, $F_{g,z}$ is much bigger than F_a and F_s as shown in section 2 of supplementary material 1. Figure 1(b) shows the distribution of calculated resultant force in vertical axis (F_z) (see section 2 in supplementary

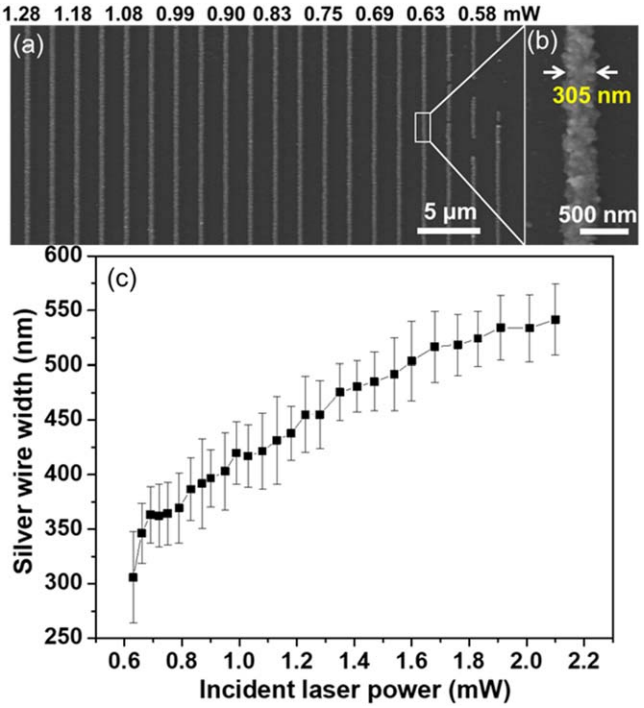

Figure 2. (a) SEM image of silver wires printed with incident laser power from 1.28 to 0.56 mW. (b) High-resolution SEM image of silver wire printed with 0.63 mW laser power. (c) Silver wire width versus incident laser power.

material 1) caused by laser light with measured power of 1 mW. The F_z is 0 N at the position of $r = 0$ nm, $z = 1$ nm. In a large volume of laser light above this point, directions of F_z are in negative z directions, and the value of the biggest F_z is 8.85×10^{-17} N at the position of $r = 0$ nm, $z = 146.2$ nm. Therefore, resultant forces in vertical direction (F_z) act as trapping forces in this volume. Figure 1(c) is the distribution of calculated resultant force in radial axis (F_r). Directions of F_r all point to the central axis of laser beam, so they are all trapping forces. The biggest F_r is 1.44×10^{-16} N at the position of $r = 110.2$ nm, $z = 0$ nm, and its value is about 2 times that of F_z. As shown in figure 1(d), new resultant forces can be caused by F_z and F_r in the volume above the point of $r = 0$ nm, $z = 1$ nm. They could propel silver nanoparticles to move to the focal spot, combine with each other and be printed on the glass substrate. Various patterns can be written on glass substrate with moving glass substrate by using the piezostage. The written sample was spray washed with ultrapure water, and characterized with a field-emission scanning electron microscopy (JEOL, JSM-7800F).

3. Results and discussions

The laser power is one of the important influence parameters for laser fabrication, so it was investigated at first. Figure 2(a) is the SEM image of silver wires printed with incident laser power from 1.28 to 0.56 mW by using FLTN. Continuous silver wire could be printed on glass substrate when the laser power was 0.63 mW or greater than that. Silver wire changed to be discontinuous when the laser power was smaller than 0.63 mW, and missing parts were getting longer and longer with the decrease of incident laser power. The silver wire printed with the incident laser power of 0.63 mW is shown in figure 2(b). Its width is about 305 nm. It is composed of sintered compacted silver nanoparticles. The largest nanoparticle on the silver wire is bigger than 50 nm, which is much bigger than that of in silver nanoparticle solution. Figure 2(c) shows the dependence of silver wire width on the incident laser power. The wire width changes nonlinearly with the decrease of laser power. The biggest standard deviation of wire width data is 41.8 nm, so the fabricated silver wire is slightly rough. In the wire printing process, trapping forces caused by laser light will help trapped nanoparticles to overcome the resistance of F_e, and combine with each other under the effect of F_v. With decrease of incident laser power, the trapping force decreases, and the volume around the laser focus where nanoparticles can be trapped and printed will also decrease. Therefore, the width of printed wire decrease with the decrease of incident laser power. Because of heating effect of the laser beam, trapped nanoparticles can be printed and sintered on the glass substrate. In this process, several nanoparticles can also be melted and combine into one nanoparticle. Therefore, nanoparticles on silver wire are bigger than just prepared nanoparticles in the solution.

The scanning speed also has significant influence on the laser trapping nanoprinting. Figure 3(a) shows silver wires printed with different scanning speeds and an incident laser power of 1.8 mW. Their scanning speeds were changed from 1 to 10 μm s^{-1}. As shown in the figure, printed silver wires have obvious distinctions in both widths and morphologies. With the scanning speed of 2 μm s^{-1} or smaller than that, silver wires were composed of the sintered compacted nanoparticles. Surfaces of these silver wires are smoother than those of silver wires printed with higher scanning speeds. With the scanning speed of 3 or 4 μm s^{-1}, printed silver wires consist of sintered nanoparticles with a lot of gaps, and their widths are bigger than those of silver wires printed with lower scanning speeds. The silver wire printed at scanning speed of 6 μm s^{-1} is rugged, and nanoparticles composing of the silver wire are melted. Many craters are found on wires printed with scanning speed of being equal to or greater than 7 μm s^{-1}, and the amount of craters increases with the increase of the scanning speed. Figure 3(b) is the dependence relation of silver wire width with the scanning speed. With scanning speeds increase from 1 to 10 μm s^{-1}, the wire width gets smaller firstly, then increases to 659 nm, and decreases to 500 nm lastly. In order to further verify the change of wire morphologies with different scanning speeds, several other groups of wires were printed with scanning speeds from 1 to 10 μm s^{-1} (figure S2 in the supplementary material 1). They all have similar change tendency in morphologies.

Silver nanoparticle in the laser light will have a position dependent velocity. It can be expressed by $v(r, z) = F(r, z)/(6\pi\mu a)$, where $F(r, z)$ is the light induced force and a is the silver nanoparticle radius [26, 27]. μ is the dynamic viscosity, and $\mu = 10^{-3}$ Pa s [26]. As shown in

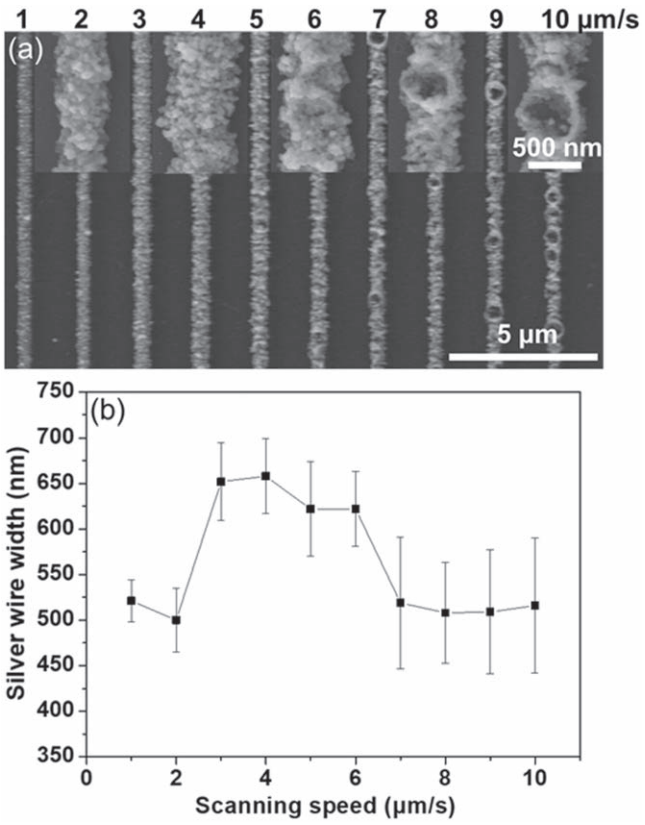

Figure 3. (a) SEM image of silver wires printed with scanning speeds from 1 to 10 μm s^{-1}. Inserted figures are the high resolution SEM image of silver wires printed with scanning speeds of 2, 4, 6, 8, and 10 μm s^{-1}. (b) Silver wire width versus laser scanning speed.

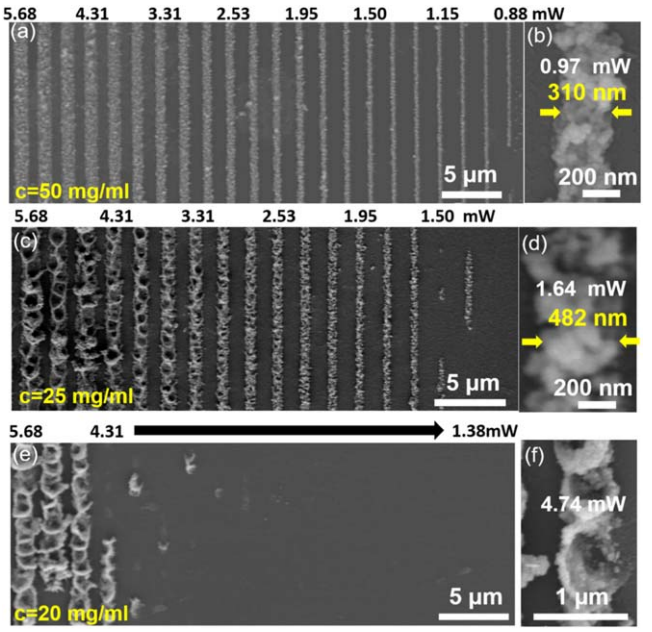

Figure 4. (a) SEM image of silver wires printed using aqueous solution with silver nanoparticle concentration of 50 mg ml^{-1}. (b) High-resolution SEM image of silver wire printed with 0.97 mW laser power. (c) SEM image of silver wires printed using aqueous solution with silver nanoparticle concentration of 25 mg ml^{-1}. (d) High-resolution SEM image of silver wire printed with 1.64 mW laser power. (e) SEM image of silver wires printed using aqueous solution with silver nanoparticle concentration of 20 mg ml^{-1}. (f) High-resolution SEM image of silver wires printed at 4.74 mW.

equation (S5), (S6), (S7) and (S8) in section 2 of supplementary material 1, the light induced force is proportional to the measured power. The biggest F_r and F_z are 2.59×10^{-16} N and 1.59×10^{-16} N with measured power of 1.8 mW, respectively. Therefore, biggest velocities of the trapped nanoparticle in radial ($v_r(r, z)$) and vertical ($v_z(r, z)$) axes are 2.12×10^{-6} m s^{-1} and 1.30×10^{-6} m s^{-1}, respectively. Velocities of the trapped particles are very slow, so only nanoparticles in a small volume above the position of $r = 0$ nm, $z = 1$ nm can move to the substrate and be printed on it.

With increase of the laser scanning speed, the interaction time of laser and nanoparticles will get shorter. The volume in which nanoparticles can be trapped and arrive the laser focal point will be reduced. Therefore, the silver wire width gets smaller with the scanning speed changed from 1 to 2 μm s^{-1}. The interaction time will further decrease with increasing of the scanning speed. In laser-nanoparticle interaction time, optical gradient force cannot gather nanoparticles tightly in the focal point, so incompact silver wire was printed with the scanning speed of 4 μm s^{-1}. Rugged morphologies of wires printed with higher scanning speeds were caused by laser induced thermal effect, and bubbles (see video of supplementary material 2) were found in the printed process with scanning speed of being equal to or greater than 7 μm s^{-1}.

Exact reasons for thermal effect increasing with scanning speed are not very clear now. We deduce that many trapped nanoparticles cannot be printed on the glass substrate immediately at higher scanning speed, and they are confined in laser focus causing much more laser absorption. Figures 4(a), (c) and (e) show SEM images of silver wires printed using aqueous solution with silver nanoparticle concentrations of 50, 25, and 20 mg ml^{-1}, respectively. Laser powers change from 5.68 to about 1 mW with scanning speed of 1 μm s^{-1}. Silver wires printed using the aqueous solution with the silver nanoparticle concentration of 50 mg ml^{-1} [figures 4(a) and (b)] were rougher than those printed using the aqueous solution with the silver nanoparticle concentration of 100 mg ml^{-1} [figures 2(a) and (b)]. However, there have no crater even for silver wire printed with laser power of 5.68 mW. It is the same as that of printed using the aqueous solution with the silver nanoparticle concentration of 100 mg ml^{-1}. The continuous fine wire printed using aqueous solution with silver nanoparticle concentration of 25 mg ml^{-1} is 482 nm, and it is also much rougher [figure 4(d)]. There are increasingly obvious craters for silver wires printed with laser power greater than 2.53 mW when used the aqueous solution with the silver nanoparticle concentration of 25 mg ml^{-1}. Only wires with craters were obtained with laser power greater 4.31 mW when used the aqueous solution with the silver nanoparticle concentration of 20 mg ml^{-1} [figures 4(e) and (f)]. Morphologies of these silver wires were similar to silver wires printed with high scanning speeds [figure 3(a)]. We deduce that it was caused by lack of nanoparticles in the solution. Trapped nanoparticles were confined in the laser focal area, but could not be printed on the substrate

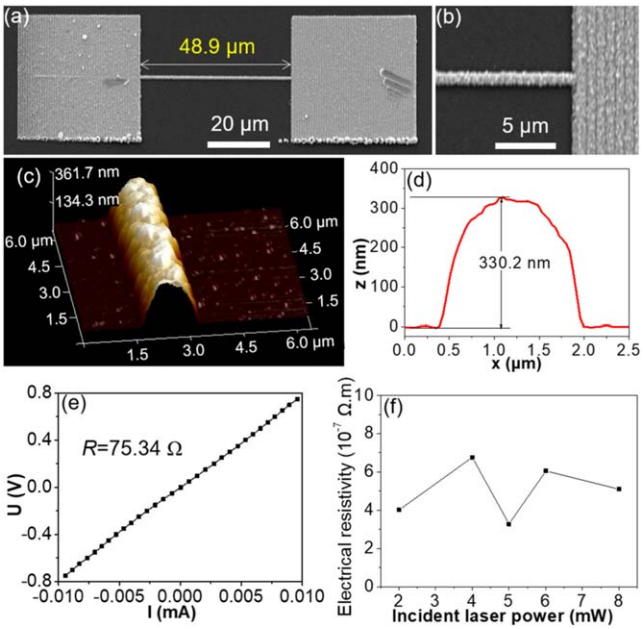

Figure 5. (a) SEM image of a silver wire and two electrode plates for resistance measurement. (b)–(d) are the high resolution SEM image, three-dimensional AFM image, and cross-section figure of the silver wire, respectively. (e) Voltage–current curve of the silver wire. (f) Electrical resistivity versus incident laser power.

immediately because of large distance between them. Therefore, they cause more laser absorption and give rise to thermal effect and bubbles.

Conductivity of the metal micro/nanowire is a very important factor for application in micro/nanoelectronics, flexible electronics, and so on. Figure 5(a) shows the silver wire and electrode plates for conductivity measurement. The length of the silver wire is 48.9 μm, and it was printed with an incident laser power of 2.04 mW and a scanning speed of 1 μm s^{-1}. In order to reduce the fabricating process, electrode plates were also printed by using FLTN. The higher resolution SEM image of the silver wire is shown in figure 5(b). The wire width is 1.13 μm. Figures 5(c) and (d) are AFM image and cross-section image of the printed silver wire, respectively. Height of the silver wire is 330.2 nm [figure 5(d)], and there are nano-undulations on the surface of the printed silver wire [figure 5(c)]. In order to obtain dimensions of the silver wire accurately, its height and width were all measured 10 times at different positions, respectively. The average height is 323 nm with a standard deviation of smaller than 19 nm. The cross-section of the printed silver wire can be seen as a small semicircle, and its area is 0.26 μm^2. Figure 5(e) shows the voltage–current curve of the printed silver wire, and resistance of the silver wire is 75.34 Ω. Therefore, the calculated electrical resistivity of this wire is 4.01 $\times$ 10^{-7} Ω m, which is 24.3 times that of bulk silver. Electrical resistivities of silver wires printed with laser power of 4, 5, 6, and 8 mW were also measured with this method. As shown in figure 5(f), the smallest and biggest resistivities are 3.28 $\times$ 10^{-7} Ω m (printed with incident laser power of 5 mW) and 6.76 $\times$ 10^{-7} Ω m (printed with incident laser power of 4 mW), respectively. However, they are in the same order of magnitude.

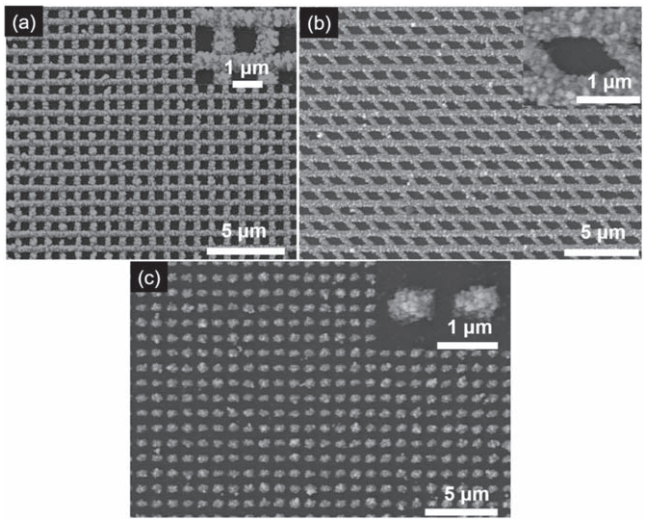

Figure 6. SEM images of (a) silver quadrate grid microstructure, (b) rhombic grid microstructure, and (c) silver dot array.

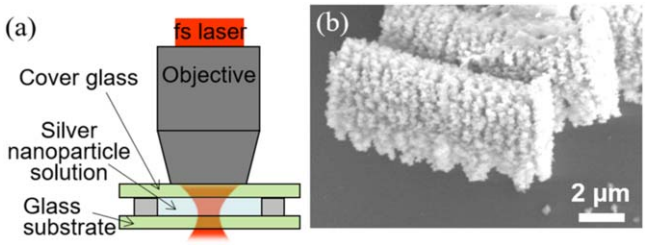

Figure 7. (a) Schematic diagram of main experimental setup for printing three-dimensional micro/nanostructure by using FLTN; (b) SEM image of printed silver cuboid structures.

Therefore, silver wires with similar resistivities but different widths can be printed by tuning the incident laser power.

Two-dimensional silver micro/nanostructures have significant applications in metamaterials, SERS, and flexible electronics. These complicated structures could well reflect the processing capability. Figure 6(a) shows a quadrate grid microstructure printed by using FLTN. The structure was fabricated with an incident laser power of 0.71 mW at a scanning speed of 1 μm s^{-1}. As shown in the high resolution image at top right corner of figure 6(a), wire widths are 446 nm for horizontal wire and 461 nm for vertical wire, respectively. Figure 6(b) is a rhombic grid microstructure printed with an incident laser power of 0.73 mW. Wire widths are 500 nm for horizontal wire and 380 nm for 45° tilted wire, respectively. A silver dot array with period of 1 μm is shown in figure 6(c). Every dot was composed of sintered nanoparticles. It was printed with an incident laser power of 1.03 mW and an exposure time of 0.8 s. These two-dimensional structures have great prospect in applications of metamaterials and SERS.

Fabrication of three-dimensional metallic micro/nanostructure is a very important and challenging work for FLTN. As shown in figure 7(a), an upright laser irradiating optical structure, which can avoid the shielding effect of the printed silver structure, was adopted to realize fabrication of three-dimensional silver micro/nanostructures by using FLTN. The

convergent laser light from the objective irradiated the cover glass, passed through the silver nanoparticle solution, and was focused on the top surface of glass substrate. Three-dimensional structures were printed on this surface layer by layer. Figure 7(b) shows tilted view of the printed silver cuboid structures. Their lengths are about 9.44 μm, and height are about 4.42 μm. They were printed with an incident laser power of 11.12 mW and a scanning speed of 6 μm s^{-1}. Their printed conditions are different from those of silver wires. It may be caused by the difference in structure of printing experimental setup.

4. Conclusions

In conclusion, silver micro/nanostructures were printed by using FLTN. Continuous silver wire with width of 305 nm was obtained, and it was composed of the sintered compacted nanoparticles. Relationships among laser power, scanning speed, nanoparticle concentration, wire width, and wire morphology were systematically studied. Morphologies of printed wires were greatly influenced by scanning speed and nanoparticle concentration. Lower scanning speed and higher silver nanoparticle concentration could help to obtain much neater silver wires. A quadrate grid microstructure, a rhombic grid microstructure, a dot array, and especially several three-dimensional cuboid microstructures were also printed by using this technology. This result provides a basis for further improving the fabrication technology of FLTN, and exhibits its potentials for fabricating two or three-dimensional structure of metamaterials, SERS, and flexible electronics.

Acknowledgments

This work was supported by the National Key Research and Development Program of China (Grant No. 2016YFA0200502), the National Natural Science Foundation of China (NSFC, Grant No. 61405196), and the CAS 'Light of West China' Program.

Data availability statement

The data that support the findings of this study are available upon reasonable request from the authors.

ORCID iDs

Hong-Zhong Cao https://orcid.org/0000-0002-2899-2414

References

[1] Lee K-S, Kim Y-S, Lee K-T and Jeong Y-H 2006 *J. Vac. Sci. Technol.* B **24** 1869–72
[2] Blasco E, Müller J, Müller P, Trouillet V, Schön M, Scherer T, Barner-Kowollik C and Wegener M 2016 *Adv. Mater.* **28** 3592–5
[3] Zarzar L D, Swartzentruber B S, Harper J C, Dunphy D R, Brinker C J, Aizenberg J and Kaehr B 2012 *J. Am. Chem. Soc.* **134** 4007–10
[4] Qian D *et al* 2018 *Opt Lett.* **43** 5335–8
[5] Fang Z, Peng Q, Song W, Hao F, Wang J, Nordlander P and Zhu X 2011 *Nano Lett.* **11** 893–7
[6] Solis D, Willingham B, Nauert S L, Slaughter L S, Olson J, Swanglap P, Paul A, Chang W-S and Link S 2012 *Nano Lett.* **12** 1349–53
[7] Cui Y, Kang L, Lan S, Rodrigues S and Cai W 2014 *Nano Lett.* **14** 1021–5
[8] Xu B-B, Zhang Y-L, Zhang W-Y, Liu X-Q, Wang J-N, Zhang X-L, Zhang D-D, Jiang H-B, Zhang R and Sun H-B 2013 *Adv. Opt. Mater.* **1** 56–60
[9] Kim J A, Wales D J, Thompson A J and Yang G-Z 2020 *Adv. Opt. Mater.* **8** 1901934
[10] Chen W T, Chen C J, Wu P C, Sun S, Zhou L, Guo G-Y, Hsiao C T, Yang K-Y, Zheludev N I and Tsai D P 2011 *Opt. Express* **19** 12837–42
[11] Kim S, Qiu F, Kim S, Ghanbari A, Moon C, Zhang L, Nelson B J and Choi H 2013 *Adv. Mater.* **25** 5863–8
[12] Ko S H, Chung J, Hotz N, Nam K-H and Grigoropoulos C P 2010 *J. Micromech. Microeng.* **20** 125010
[13] Höflich K, Yang R B, Berger A, Leuchs G and Christiansen S 2011 *Adv. Mater.* **23** 2657–61
[14] Kuo W-S, Lien C-H, Cho K-C, Chang C-Y, Lin C-Y, Huang L L H, Campagnola P J, Dong C Y and Chen S-J 2010 *Opt. Express* **18** 27550–9
[15] Masui K, Shoji S, Asaba K, Rodgers T C, Jin F, Duan X-M and Kawata S 2011 *Opt. Express* **19** 22786–96
[16] Cao Y-Y, Takeyasu N, Tanaka T, Duan X-M and Kawata S 2009 *Small* **5** 1144–8
[17] Barton P, Mukherjee S, Prabha J, Boudouris B W, Pan L and Xu X 2017 *Nanotechnology* **28** 505302
[18] Bahns J T, Sankaranarayanan S K R S, Giebink N C, Xiong H and Gray S K 2012 *Adv. Mater.* **24** OP242–6
[19] Xu B-B, Zhang R, Wang H, Liu X-Q, Wang L, Ma Z-C, Chen Q-D, Xiao X-Z, Han B and Sun H-B 2012 *Nanoscale* **4** 6955–8
[20] Wang H, Liu S, Zhang Y-L, Wang J-N, Wang L, Xia H, Chen Q-D, Ding H and Sun H-B 2015 *Sci. Technol. Adv. Mater.* **16** 024805
[21] Qiu M, Zhang L, Tang Z, Jin W, Qiu C-W and Lei D Y 2018 *Adv. Funct. Mater.* **28** 1803147
[22] Hou Y H, Liu B, Liu Y, Zhou Y H, Song T T, Zhou Q, Sha G and Yan M 2019 *Opto-Electron. Adv.* **2** 180028
[23] Ahn B Y, Duoss E B, Motala M J, Guo X, Park S-I, Xiong Y, Yoon J, Nuzzo R G, Rogers J A and Lewis J A 2009 *Science* **323** 1590–3
[24] Usman A, Chiang W-Y and Mashuhara H 2013 *Sci. Prog.* **96** 1–18
[25] Svoboda K and Block S M 1994 *Opt. Lett.* **19** 930–2
[26] Gargiulo J, Violi I L, Cerrotta S, Chvátal L, Cortes E, Perassi E M, Diaz F, Zemanek P and Stefani F D 2017 *ACS Nano* **11** 9678–88
[27] Melzer J E and McLeod E 2018 *ACS Nano* **12** 2440–7